

Cite this: DOI: 00.0000/xxxxxxxxxx

## Tuning the Surface Properties of AuPd Nanoparticles for Adsorption of O and CO

Ilya V. Chepkasov,<sup>\*ab</sup> Ivan S. Zamulin,<sup>b</sup>, Viktor S. Baidyshev<sup>a</sup> and Alexander G. Kvashnin<sup>a</sup>

Received Date

Accepted Date

DOI: 00.0000/xxxxxxxxxx

Bimetallic nanoparticles are attracting increasing attention as effective catalysts because they can exhibit higher efficiencies than their monometallic counterparts. Recent studies show that PdAu nanoparticles can exhibit truly impressive catalytic activity, due to the synergistic effect of their properties. However, fine-tuning of the catalytic activity requires understanding of the full picture of the processes occurring in bimetallic particles of different compositions and structures. Here we study the influence of the structure and composition of PdAu nanoparticles on the electronic properties, charge distribution and adsorption properties (CO and O) using *ab initio* calculations. Two types of nanoparticles were considered: core-shell (Pd@Au, Au@Pd) and bimetallic alloy (Au-Pd) with an average diameter of 2 nm (321 atoms) having either fcc or icosahedral structures. The results obtained on surface charges show the possibility of fine-tuning the surface properties of nanoparticles by changing the atomic structure and composition. Additionally the adsorption of O and CO on the surface of PdAu nanoparticles with fcc structure type has been studied. The obtained adsorption data correlates with surface charge redistribution and the *d*-band center. The results of this study thus open up great prospects for tuning the catalytic properties of nanocatalysts by modifying their local atomic environment.

### 1 Introduction

The catalytic activity of gold nanoparticles with respect to the oxidation of carbon monoxide at low temperatures was discovered by Haruta<sup>1</sup> in 1987. This discovery has attracted a great interest to gold nanocatalysts as they violated the traditional view that gold has no catalytic activity. Discovered nanoparticles have small size less than 5 nm<sup>1</sup>, which was important for the efficiency of heterogeneous catalysis on oxide substrates.

Progress in the synthesis of noble metal nanoparticles made it possible to actively study their catalytic activity<sup>2,3</sup>. In particular, it was shown that Pd nanoparticles of 2-3 nm are effective in heterogeneous catalysis<sup>4</sup>. Au nanoparticles can be used as catalysts for photocatalytic splitting of water under the influence of solar energy, CO<sub>2</sub> reduction, and decomposition of organic pollutants<sup>5</sup>.

Bimetallic catalysts based on PdAu nanoparticles have increased catalytic activity due to the synergistic effect. The synergistic effect occurs when two catalytically active metals are combined in such a way that the catalytic efficiency exceeds that of their monometallic counterparts<sup>6</sup>. This makes bimetal-

lic nanoparticles an interesting class of materials for catalysis in various chemical processes<sup>7</sup>. Combination of Pd with less active and more selective metal, such as Au, one can form core-shell nanoparticles. The catalytic efficiency of core-shell nanoparticles can be increased more than ten times compared to their monometallic counterparts<sup>8-11</sup>. The following factors are responsible for this effect. First of all, charge redistribution at the core-shell interface and the appearance of a dimensional quantum effect in the case of a atomic-thin shell<sup>9,12</sup>. Another important factor is the deformation of the metallic shell due to the lattice mismatch between core and shell leading to changes in the electronic properties<sup>13</sup>. Recent work by Zhang et al.<sup>11</sup> has shown that selecting the specific sizes of core and shell of Au@Pd nanoparticles leads to significant increase in the catalytic activity. However, such tuning of the nanoparticle properties requires a detailed understanding of the processes occurring at the core-shell interface and on the nanoparticle surface. The development of numerical methods, namely density functional theory, makes it possible to obtain all the necessary information about nanoparticles from the simulations.

To estimate the catalytic efficiency of nanoparticles without direct calculations of the adsorption of certain atoms and molecules there are a number of models that provide information on the reactivity of nanoparticles<sup>14,15</sup>. The most successful model was proposed by Hammer and Nørskov<sup>15</sup>, called the *d*-band model. It justifies the reactivity of transition metals based on a single

<sup>a</sup> Skolkovo Institute of Science and Technology, Bolshoy Boulevard 30, bld. 1, Moscow 121205, Russian Federation; E-mail: I.Chepkasov@skoltech.ru

<sup>b</sup> Katanov Khakass State University, 90 Lenin pr, 655017, Abakan, Russian Federation

† Electronic Supplementary Information (ESI) available: [details of any supplementary information available should be included here]. See DOI: 10.1039/cXCP00000x/

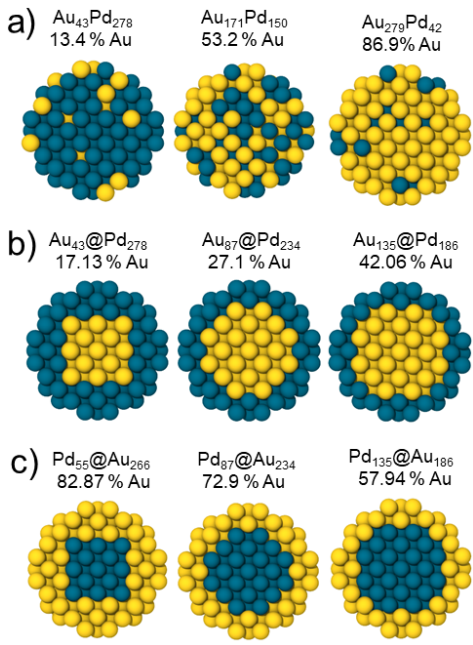


Fig. 1 Atomic structures of the considered bimetallic fcc AuPd nanoparticles with different local environments, namely a) bimetallic alloy, b) Au@Pd, and c) Pd@Au.

parameter, the center of the *d*-band of the surface atoms. This model well describes the difference in the adsorption energy of atoms and molecules on different parts of the nanoparticle surface. In addition to the electronic structure, the study of the surface charge redistribution can also provide important information on the catalytic activity of nanoparticles<sup>14</sup>.

Here we considered three different types of PdAu bimetallic nanoparticles, namely Pd-core/Au-shell (Pd@Au), Au-core/Pd-shell (Au@Pd), and bimetallic alloy (Au-Pd) particles to study influence of particle structure on the surface properties, i.e. electronic structure and charge. For nanoparticles with fcc structure, the adsorption energies of CO molecules and O atoms on the PdAu nanoparticles with different compositions were also estimated.

## 2 Simulation methodology

To analyze the electronic structure and surface charge of nanoparticles using the density functional theory (DFT)<sup>16,17</sup>, we first optimized the geometry of each studied nanoparticle. The generalized gradient approximation (GGA) was used with the revised PBE<sup>18</sup> parametrization for the exchange-correlation functional as implemented in the VASP software package<sup>19–21</sup>. Ion-electron interaction was described by the projector augmented-plane-waves method (PAW)<sup>22</sup> with cut-off energy of 480 eV. The orbital occupancies were smeared using the first-order Methfessel-Paxton method with the smearing width of 0.05 eV. The local geometry optimization of considered clusters was conducted until the maximum force on each atom became less than 0.03 eV/Å. The nanoparticles were placed in a box with a vacuum of at least 10 Å separating them.

Spin-polarized Generalised Gradient Approximation (GGA)

with the PBE parametrization was used to calculate adsorption energies. The energy of the oxygen molecule was calculated for the triplet state using spin-polarized calculations. Effective interaction between the valence electrons and nuclei screened by frozen core electrons was described via Scalar Relativistic Ultra-soft Pseudopotentials. The integration of spin-orbit coupling with scalar relativistic pseudopotentials through the implementation of the VASP code resulted in fully relativistic results. This outcome holds significance for nanoparticles that are composed of gold. Grimme correction (DFT-D3)<sup>23</sup> was applied to take into account dispersive van der Waals interaction.

The results of the calculations were post-processed and visualized using the Open Visualization Tool (OVITO)<sup>24</sup> and VESTA package<sup>25,26</sup>. Electron transfer was explored by Bader analysis<sup>27</sup>. To determine the structural stability, the excess energy<sup>28</sup> of nanoparticles was calculated with respect to a bulk.

$$\Delta = (E_{NP_s} - E_{Au}N_{Au} - E_{Pd}N_{Pd}) / (N_{Au} + N_{Pd})^{2/3}, \quad (1)$$

where  $E_{NP_s}$  is the energy of the considered nanoparticle,  $N_{Au}$  and  $N_{Pd}$  correspond to the number of Pd and Au atoms, respectively, and  $E_{Au}$  and  $E_{Pd}$  are the energies per atom for the bulk Pd and Au respectively.

Adsorption energies of CO molecules and O atoms were calculated as

$$E_{ads}[CO] = E[CO/Au_xPd_y] - E[CO] - E[Au_xPd_y], \quad (2)$$

$$E_{ads}[O] = E[O/Au_xPd_y] - E[O_2]/2 - E[Au_xPd_y], \quad (3)$$

where  $E[CO/Au_xPd_y]$  and  $E[O/Au_xPd_y]$  are the energies of adsorption complexes of CO and O on  $Au_xPd_y$  nanoparticles, while  $E[CO]$ ,  $E[O_2]$ , and  $E[Au_xPd_y]$  are the energies of the gas phase CO and  $O_2$  molecules, and the considered  $Au_xPd_y$  nanoparticles respectively.

## 3 Results and discussion

Our study is devoted to identification of the peculiarities corresponding to the influence of the structure type, local atomic environment, and composition of PdAu nanoparticles on their surface properties. We considered core-shell and bimetallic alloy AuPd NPs with the diameter of 2 nm (321 atoms) having either fcc, icosahedral or amorphous structures. This is the smallest size that can be experimentally obtained for PdAu nanoparticles<sup>10</sup>. From another perspective, this size allowed us to perform calculations with a good trade-off between computation and detection in experiments. AuPd nanoparticles with fcc structure are shown in Fig. 1. For core-shell Pd@Au and Au@Pd nanoparticles only compositions in which the entire surface consists of Au or Pd atoms, respectively, were considered. Whereas there is no restrictions for composition in the case of bimetallic alloys (Au-Pd). To compare the results for the bimetallic alloy, we also considered the L1<sub>1</sub> PdAu alloy. We considered different structures of AuPd (fcc and Ih) because particles with fcc and Ih structures have been experimentally synthesized<sup>11,29</sup>. The amorphous structure was chosen because nanoparticles can be used in high-temperature

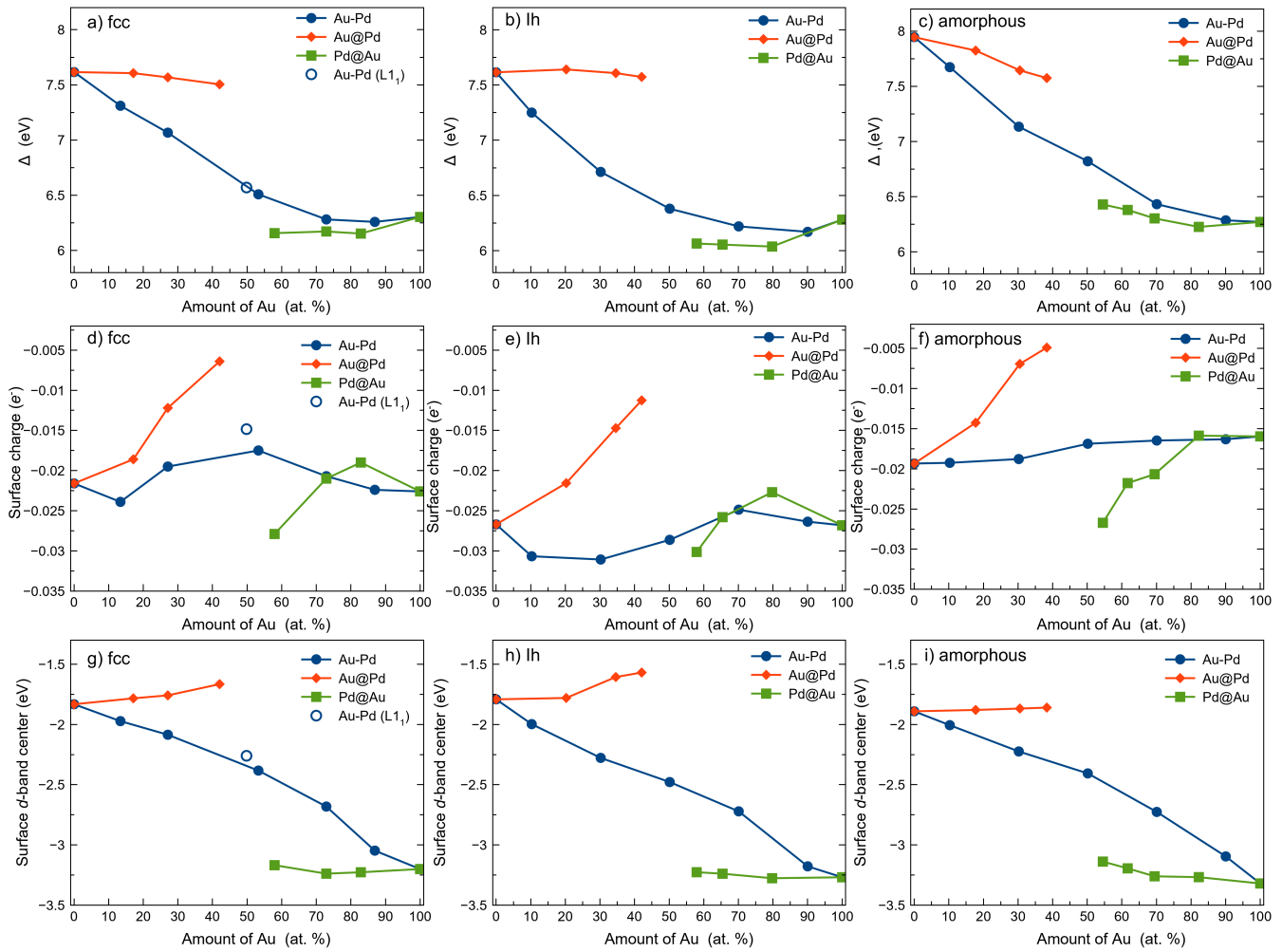


Fig. 2 (a,b,c) Excess energies  $\Delta$ , (d,e,f) Average surface charge and (g,h,i) Average d-band centers of AuPd NPs with different structure types (fcc, Ih, amorphous) and atomic environment (Pd@Au, Au@Pd, Au-Pd) as a function of composition. Positive values of charge mean deficiency of electrons (electrons have gone from the surface inside), negative values denote excess of electrons resulting in negative surface charge.

catalysis when the closest packed structure of nanoparticle can change to amorphous structure<sup>30–34</sup>. Amorphous nanoparticles were obtained by MD modeling the fcc melting of AuPd nanoparticles and rapid freezing of the amorphous structure.

The dependence of  $\Delta$  on the Au concentration in Au-Pd, Pd@Au, and Au@Pd nanoparticles with different structures (fcc, Ih and amorphous) are shown in Fig. 2(a-c). Significantly different behaviour were observed for two types of core-shell nanoparticles. Au@Pd nanoparticles are energetically less favorable than other structures, which has also been experimentally and theoretically observed<sup>35–38,38</sup>. This comes from the surface energies of Pd and Au, determined to be 1.74 and 1.33 J/m<sup>2</sup>, respectively<sup>39</sup>. The Au surface is more favorable than Pd leading to stabilization of Pd@Au nanoparticles, see green line in Fig. 2 (a-c).

One of the main driving forces of adsorption of various chemical agents on the surface is uncompensated surface charge arising from the presence of broken bonds on the nanoparticle surface. We studied the surface charge distribution by using the Bader method<sup>27</sup>, as shown in in Fig. 2 (d-f). It can be noted

that homogeneous Au-Pd alloys always have an excessive negative charge from -0.016 to -0.03 e<sup>-</sup>. Depending on the type of metal in the shell/core, there is a different excess of electrons on the surface. For Pd@Au nanoparticles, the surface is more negatively charged (to -0.03 e<sup>-</sup>), for Au@Pd the surface is less negatively charged (to -0.005 e<sup>-</sup>). The effect of charge redistribution in bimetallic nanoparticles was previously studied for the case of PtPd and CuAu nanoparticles<sup>40,41</sup>. This effect was observed for PdAu nanoparticles because Au has a smaller work function compared to Pd. This can be seen most clearly seen from the Fig. 3(a,b) in the case of Au@Pd nanoparticles, where we can clearly see the localization of the electron density being shifted from the Pd atoms to the region close to the subsurface Au atoms. In the opposite situation of Pd@Au we observed less charge distribution (Fig.3c,d). Charge redistribution effect should be taken into account considering the application of nanoparticles in catalysis, since different molecules require different charges on the surface for adsorption. In particular, CO molecule adsorbs by the donor mechanism<sup>42,43</sup> and it requires positively charged sites for the

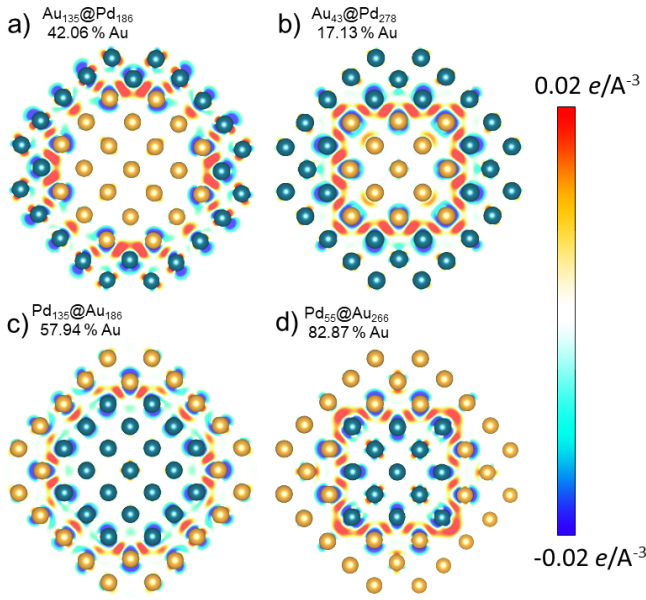


Fig. 3 Charge transfer between Pd and Au atoms in Pd@Au, Au@Pd nanoparticles visualized as a difference between the electron density of core and shell. Red areas correspond to density build-up, blue to depletion. (For interpretation of the references to color in this figure legend, the reader is referred to the web version of this article). The Pd and Au atoms are depicted as dark blue and yellow spheres, respectively.

adsorption. Thus, by changing the structure and composition of nanoparticles one can finely change the redistribution of the surface charge, which opens great prospects for their use in various applications.

We calculated the *d*-band centers (as one of the most successful descriptors for determination of catalytic properties) for all considered nanoparticles by calculating the projected densities of states (pDOS). Only the surface atoms were selected for the analysis and the average value of the *d*-band centers among all surface atoms was calculated as shown in Fig. 2 (g-i). The average values of the *d*-band centers on the surface of pure Au nanoparticle, are -3.20, -3.26 and 3.32 eV for fcc, Ih and amorphous respectively. In the case of pure Pd it is -1.83, 1.79 and 1.89 eV for fcc, Ih and amorphous. As one can see from Fig. 2 (g-i) the structure of nanoparticle (fcc, Ih or amorphous) does not significantly affect on the calculated *d*-band centers. For Au@Pd nanoparticles, the maximum values are -1.66, -1.56 and 1.85 eV for the fcc, Ih and amorphous structure, respectively, see red line in Fig. 2(g-i). Pd@Au nanoparticles showed minimum values of the *d*-band centers of -3.23, -3.27 and 3.26 eV for the fcc, Ih and amorphous structure, respectively, see green line in Fig. 2(g-h). Bimetallic alloy particles show an almost monotonic decrease in the *d*-band center depending on the Au concentration (blue line in Fig. 3), due to the decreasing number of Au atoms in the surface, resulting in a monotonic change in electronic properties from Pd to Au. As shown in Ref<sup>44</sup>, the smaller the value of the *d*-band centers, the weaker the adsorbent binding energy to the metal surface. However, according to the Sabatier principle, the adsorption energy must be neither too strong nor too weak for the adsorbent to interact with the catalyst surface. Thus, a change in the ratio

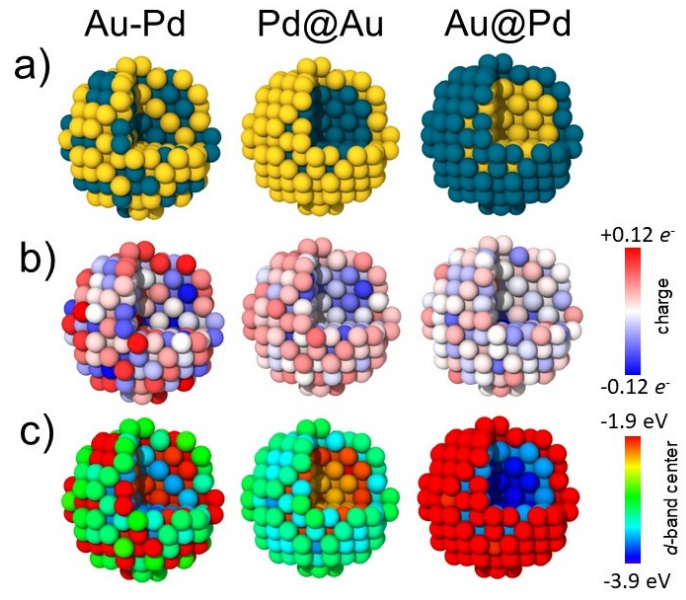


Fig. 4 a) Atomic structures of bimetallic fcc AuPd nanoparticles with different atomic environment, b) distribution of atomic charge, c) distribution of *d*-band centers

of the core-shell atoms in PdAu nanoparticles can lead to significant changes in the surface properties. In particular, a shift of the *d*-band center with subsequent change in the catalytic activity of the nanoparticle surface. Fig. 4 demonstrates how the charge and the *d*-band centers are redistributed across the nanoparticles with different structures. Results on the excess energy, average surface charge and surface *d*-band center for L1<sub>1</sub> PdAu nanoparticle close to the results of bimetallic alloy nanoparticles, see Fig. 2. The atomic structure of L1<sub>1</sub> PdAu nanoparticle is presented in Supporting Information

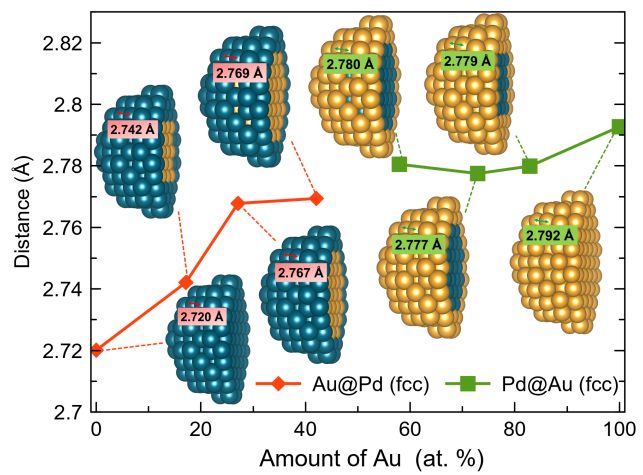


Fig. 5 Interatomic distance between surface atoms of considered clusters depending on the composition.

The behavior of the surface charge and the *d*-band center as a function of the composition can be explained by the variation of the shell lattice parameter depending on the core in the nanopar-

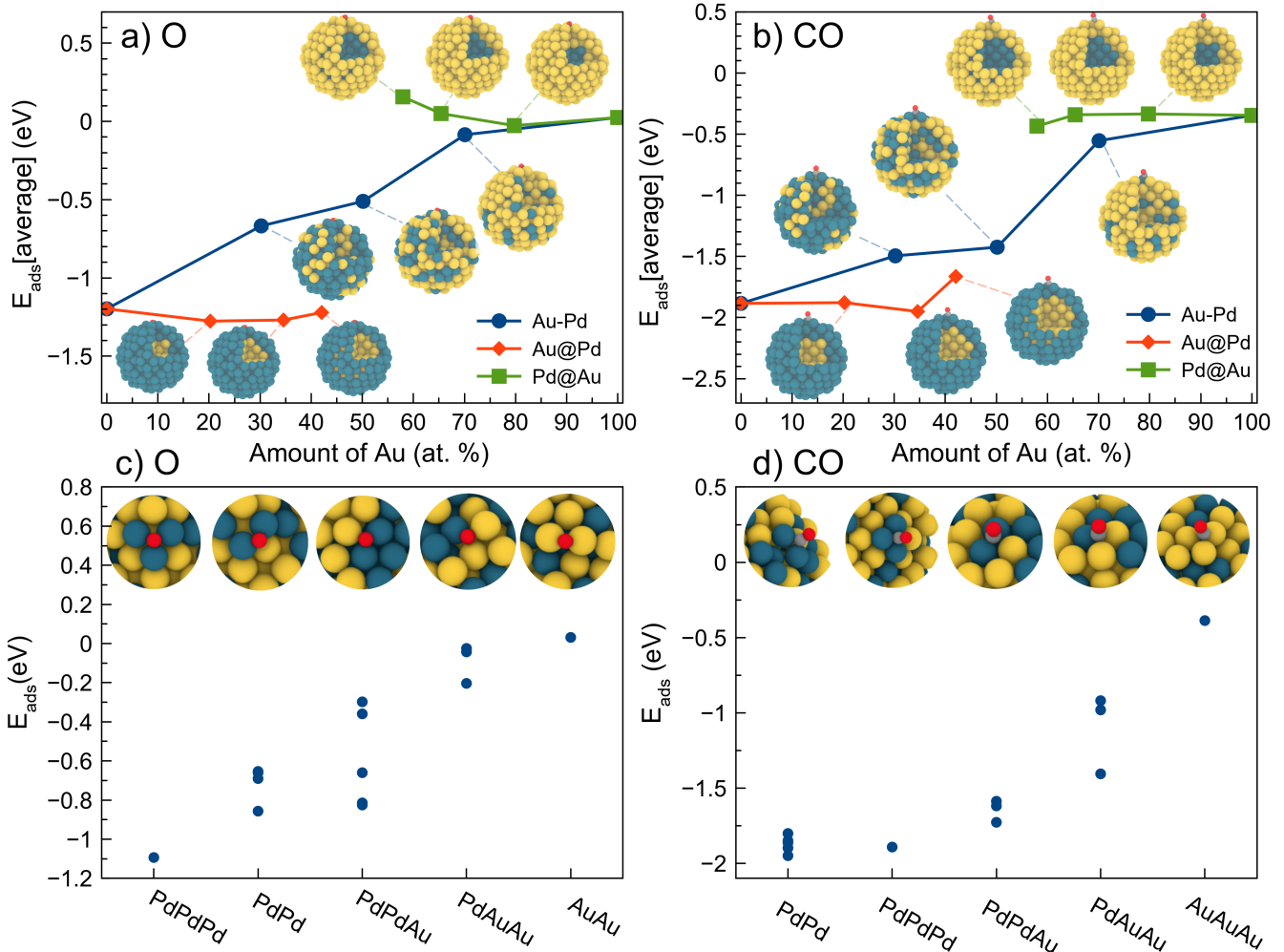


Fig. 6 (a,b) Average adsorption energy of O and CO on PdAu NPs with different local atomic environment (Pd@Au, Au@Pd, Pd-Au) as a function of composition. (c, d) Binding energies of O atoms and CO molecules on the considered bimetallic Pd-Au alloy (50% Pd, 50% Au) nanoparticle for various compositions and adsorption sites. The Pd and Au atoms are depicted as dark blue and yellow spheres, respectively.

ticle. For example Guan et al.<sup>45</sup> used DFT to study how the lattice parameters and electronic properties of the Pt monolayer on the Au substrate change (1ML-Pt/Au(111)). It was clearly showed that the underlying gold expands the lattice of the supported platinum layer by 4.3% from 2.77 to 2.89 Å. This lattice expansion and the orbital hybridization between platinum and gold induce a significant up-shift of the platinum 5d-band center by 0.69 eV towards the Fermi level. Shifted d-band center would make the exposed platinum overlayer more reactive. The tendency of changing the interatomic distance in the shell in Au@Pd nanoparticles was also shown earlier by Zhang et al.<sup>11</sup>. In our work, we also studied the change of interatomic distance on the nanoparticle surface depending on the composition in core and shell. For Pd the interatomic distance changes from 2.720 Å for pure Pd nanoparticle to 2.769 Å for Au<sub>135</sub>@Pd<sub>186</sub> (42.06 % Au) nanoparticle. In the case of Pd@Au nanoparticles the interatomic distance on the surface changes from 2.792 Å for pure Au nanoparticle to 2.780 Å for Pd<sub>135</sub>@Au<sub>186</sub> (57.94 % Au) nanoparticle (Fig. 5). These changes in the interatomic distance are one of the factors leading to changes in the surface properties of core-shell nanopar-

ticles.

The next part of the study is devoted to the investigation of the adsorption of O and CO on the NPs. We chose the fcc structure type as a model system for this study, which allows us to show the general tendencies in the adsorption of O and CO on the PdAu NPs. In order to determine the influence of the local atomic environment of PdAu NPs on the adsorption energy of O and CO, we considered 14 different adsorption sites (including top, bridge, hollow, and kink) on the surface of PdAu nanoparticles with fcc structure. For Pd nanoparticles, the average adsorption energy of CO was -1.88 eV, demonstrating good agreement with previous works<sup>46–49</sup>. For Au nanoparticles the average adsorption energy of CO was -0.34 eV which good agreement with previous works<sup>50</sup>. The adsorption energies of O and CO on the surface of Au@Pd nanoparticles are lower than those for Pd@Au nanoparticles with Au surface (Fig. 6a,b). When altering the size ratio of the core and shell, there are minor fluctuations observed in the energy of adsorption for both O and CO. More information about adsorption positions and adsorption energies are more presented in SI. In the case of the bimetallic alloy NP, the adsorption energy

will strongly depend on the type of adsorption site (the variety of compositions is greater compared to pure metal surfaces). For example in Fig. 6c,d we have shown the dependence of the adsorption energy on the type of adsorption site. The site which consisting only of Pd atoms binds O and CO more strongly than mixed Pd-Au sites, whereas pure Au sites are not locally stable for the adsorption of these species.

## 4 Conclusions

We have performed the *ab initio* calculations to systematically investigate the influence of structural peculiarities of AuPd nanoparticles of 2 nm diameter (321 atoms) on electronic properties. The type of core-shell nanoparticles (Pd@Au and Au@Pd) as well as the thickness of the shell with respect to the core were found to be responsible for significant surface charge redistribution. Pd nanoparticles with atomic-thick Au shell (Pd@Au) exhibit a significant excess of electrons flowing from the Pd core to the Au surface, forming a negative charge on the surface, suitable for O<sub>2</sub> adsorption. The type of structure (fcc or Ih) of the core-shell nanoparticles has almost no effect on the surface charge. For bimetallic alloy nanoparticles the surface charge is independent to the change in all structural characteristics (composition, local atomic environment, and structure type). The calculated *d*-band centers for all considered nanoparticles shows possibility to adjust catalytic properties by changing the structure. The smaller the value of the *d*-band centers, the stronger the binding energy of the adsorbents to the metal surface. The adsorption of O and CO on the surface of PdAu nanoparticles with fcc structure type has been studied in detail by considering 14 symmetrical non-equivalent adsorption sites. Alloy bimetallic fcc nanoparticles show a much broader distribution of adsorption energies for both O and CO adsorption. The obtained data correlate with the change in surface charge and *d*-band center. Thus, the results of this study open great prospects for tuning the catalytic properties of nanocatalysts by modifying their local atomic environment.

## Author Contributions

Conceptualization: I.V.C. Writing – original draft: I.V.C., I.S.V., A.G.K. Investigation: I.V.C., I.S.Z., V.S.B. Writing – review & editing: A.G.K., I.V.C. Supervision: A.G.K.

## Conflicts of interest

There are no conflicts to declare.

## Acknowledgements

The study was supported by the Russian Science Foundation grant No. 19-72-30043. The research is carried out using resources of the Center for the Information and Computing of Novosibirsk State University.

## Notes and references

- 1 M. Haruta, T. Kobayashi, H. Sano and N. Yamada, *Chemistry Letters*, 1987, **16**, 405–408.
- 2 A. S. Konopatsky, D. V. Leybo, K. L. Firestein, I. V. Chepkasov, Z. I. Popov, E. S. Permyakova, I. N. Volkov, A. M. Kovalskii, A. T. Matveev, D. V. Shtansky *et al.*, *ChemCatChem*, 2020, **12**, 1691–1698.
- 3 A. M. Kovalskii, I. N. Volkov, N. D. Evdokimenko, O. P. Tkachenko, D. V. Leybo, I. V. Chepkasov, Z. I. Popov, A. T. Matveev, A. Manakhov, E. S. Permyakova *et al.*, *Applied Catalysis B: Environmental*, 2022, **303**, 120891.
- 4 M. T. Reetz and J. G. De Vries, *Chemical Communications*, 2004, 1559–1563.
- 5 X. Liu, J. Iocozzia, Y. Wang, X. Cui, Y. Chen, S. Zhao, Z. Li and Z. Lin, *Energy & Environmental Science*, 2017, **10**, 402–434.
- 6 L. Zhang, M. Zhou, A. Wang and T. Zhang, *Chemical reviews*, 2019, **120**, 683–733.
- 7 W.-Y. Yu, G. M. Mullen and C. B. Mullins, *The Journal of Physical Chemistry C*, 2013, **117**, 19535–19543.
- 8 X. Huang, O. Akdim, M. Douthwaite, K. Wang, L. Zhao, R. J. Lewis, S. Pattisson, I. T. Daniel, P. J. Miedziak, G. Shaw *et al.*, *Nature*, 2022, **603**, 271–275.
- 9 J. E. van der Hoeven, J. Jelic, L. A. Olthof, G. Totarella, R. J. van Dijk-Moes, J.-M. Krafft, C. Louis, F. Studt, A. van Blaaderen and P. E. de Jongh, *Nature Materials*, 2021, **20**, 1216–1220.
- 10 X. Zhu, Q. Guo, Y. Sun, S. Chen, J.-Q. Wang, M. Wu, W. Fu, Y. Tang, X. Duan, D. Chen *et al.*, *Nature communications*, 2019, **10**, 1428.
- 11 X. Zhang, Z. Sun, R. Jin, C. Zhu, C. Zhao, Y. Lin, Q. Guan, L. Cao, H. Wang, S. Li *et al.*, *Nature Communications*, 2023, **14**, 530.
- 12 P. Strasser, S. Koh, T. Anniyev, J. Greeley, K. More, C. Yu, Z. Liu, S. Kaya, D. Nordlund, H. Ogasawara *et al.*, *Nature chemistry*, 2010, **2**, 454–460.
- 13 M. Luo and S. Guo, *Nature Reviews Materials*, 2017, **2**, 1–13.
- 14 S. Zha, Z.-J. Zhao, S. Chen, S. Liu, T. Liu, F. Studt and J. Gong, *CCS Chemistry*, 2020, **2**, 262–270.
- 15 B. Hammer and J. K. Nørskov, *Advances in catalysis*, Elsevier, 2000, vol. 45, pp. 71–129.
- 16 L. J. Sham and W. Kohn, *Physical Review*, 1966, **145**, 561.
- 17 P. Hohenberg and W. Kohn, *Physical Review*, 1964, **136**, B864.
- 18 B. Hammer, L. B. Hansen and J. K. Nørskov, *Physical Review B*, 1999, **59**, 7413.
- 19 G. Kresse and J. Hafner, *Journal of Physics: Condensed Matter*, 1994, **6**, 8245.
- 20 G. Kresse and J. Hafner, *Physical Review B*, 1994, **49**, 14251.
- 21 G. Kresse and J. Furthmüller, *Physical review B*, 1996, **54**, 11169.
- 22 P. E. Blöchl, *Physical review B*, 1994, **50**, 17953.
- 23 S. Grimme, J. Antony, S. Ehrlich and H. Krieg, *The Journal of Chemical Physics*, 2010, **132**, 154104.
- 24 A. Stukowski, *Modelling and Simulation in Materials Science and Engineering*, 2009, **18**, 015012.
- 25 K. Momma and F. Izumi, *Journal of Applied Crystallography*, 2008, **41**, 653–658.
- 26 K. Momma and F. Izumi, *Journal of Applied Crystallography*, 2011, **44**, 1272–1276.
- 27 W. Tang, E. Sanville and G. Henkelman, *Journal of Physics: Condensed Matter*, 2009, **21**, 084204.

- 28 R. Ferrando, G. Rossi, A. C. Levi, Z. Kuntová, F. Nita, A. Jelea, C. Mottet, G. Barcaro, A. Fortunelli and J. Goniakowski, *The Journal of chemical physics*, 2009, **130**, year.
- 29 T. Lv, X. Yang, Y. Zheng, H. Huang, L. Zhang, J. Tao, L. Pan and Y. Xia, *The Journal of Physical Chemistry C*, 2016, **120**, 20768–20774.
- 30 Y. Y. Gafner, S. Gafner and I. Chepkasov, *Journal of Experimental and Theoretical Physics*, 2010, **111**, 608–618.
- 31 I. Chepkasov, Y. Y. Gafner and S. Gafner, *Journal of Aerosol Science*, 2016, **91**, 33–42.
- 32 I. V. Chepkasov, Y. Y. Gafner, M. Vysotin and L. Redel', *Physics of the Solid State*, 2017, **59**, 2076–2081.
- 33 I. Chepkasov, Y. Y. Gafner and S. Gafner, *Phase Transitions*, 2017, **90**, 590–597.
- 34 I. Chepkasov, Y. Y. Gafner, S. Gafner and S. Bardahanov, *The Physics of Metals and Metallography*, 2016, **117**, 1003–1012.
- 35 Y. Ding, F. Fan, Z. Tian and Z. L. Wang, *Journal of the American Chemical Society*, 2010, **132**, 12480–12486.
- 36 J. A. Boscoboinik, C. Plaisance, M. Neurock and W. T. Tysoe, *Physical Review B*, 2008, **77**, 045422.
- 37 D. Yuan, X. Gong and R. Wu, *Physical Review B*, 2008, **78**, 035441.
- 38 H. Liu, U. Pal, R. Perez and J. Ascencio, *The Journal of Physical Chemistry B*, 2006, **110**, 5191–5195.
- 39 W. Tyson and W. Miller, *Surface Science*, 1977, **62**, 267–276.
- 40 I. Chepkasov, M. Visotin, E. Kovaleva, A. Manakhov, V. Baidyshev and Z. Popov, *The Journal of Physical Chemistry C*, 2018, **122**, 18070–18076.
- 41 I. V. Chepkasov, V. S. Baidyshev, A. A. Golubnichiy, I. S. Zamulin, A. G. Kvashnin and S. M. Kozlov, *Aggregate*, 2022, **3**, e273.
- 42 X.-N. Li, Z. Yuan and S.-G. He, *Journal of the American Chemical Society*, 2014, **136**, 3617–3623.
- 43 J.-J. Chen, X.-N. Li, Q. Chen, Q.-Y. Liu, L.-X. Jiang and S.-G. He, *Journal of the American Chemical Society*, 2018, **141**, 2027–2034.
- 44 S. Jiao, X. Fu and H. Huang, *Advanced Functional Materials*, 2022, **32**, 2107651.
- 45 Q. Guan, C. Zhu, Y. Lin, E. I. Vovk, X. Zhou, Y. Yang, H. Yu, L. Cao, H. Wang, X. Zhang *et al.*, *Nature Catalysis*, 2021, **4**, 840–849.
- 46 H. Y. Kim and G. Henkelman, *ACS Catalysis*, 2013, **3**, 2541–2546.
- 47 I. V. Yudanov, R. Sahnoun, K. M. Neyman, N. Rösch, J. Hoffmann, S. Schauermann, V. Johaneck, H. Unterhalt, G. Rupprechter, J. Libuda *et al.*, *The Journal of Physical Chemistry B*, 2003, **107**, 255–264.
- 48 J. B. Davis, F. Baletto and R. L. Johnston, *The Journal of Physical Chemistry A*, 2015, **119**, 9703–9709.
- 49 M. Mamatzkulov, I. V. Yudanov, A. V. Bukhtiyarov, I. P. Prosvirin, V. I. Bukhtiyarov and K. M. Neyman, *The Journal of Physical Chemistry C*, 2018, **123**, 8037–8046.
- 50 W. McKee, M. Patterson, D. Huang, J. Frick, R. Kurtz, P. Sprunger, L. Liu and Y. Xu, *The Journal of Physical Chemistry C*, 2016, **120**, 10909–10918.